HEFAT2014
10th International Conference on Heat Transfer, Fluid Mechanics and Thermodynamics
14 – 16 July 2014
Orlando, Florida

DYNAMIC FORCES AND ACOUSTIC ENERGY DISSIPATION IN CONICAL BUBBLE LUMINESCENCE

[1]Navarrete M.,* [2]Castellanos F., [3]Naude F., and [3]Méndez F.
*Author for correspondence
[1]Instituto de Ingeniería, Universidad Nacional Autónoma de México, D.F.,
[3]Facultad de Ingeniería, Universidad Nacional Autónoma de México, D.F.,
Av. Universidad 3000,
[2]Instituto Politécnico Nacional, IPN, CIIDIR Oaxaca,
México,
E-mail: mnm@pumas.iingen.unam.mx.

ABSTRACT

The dynamics and acoustics of conical bubble collapse occurring in a U-Tube device are studied. Two conical shapes are used, one with a smooth interior and another with a stepped interior in order to understand their associated phenomena such as: luminescence, bubble cloud formation, and emission of strong rebound pressures. High-speed video frames, waveforms from piezoelectric transducers and photomultipliers were acquired during the experimental runs. All data are synchronized on the same timeline. To explore the details of the acoustic energy dissipation, the piezoelectric waveforms were analyzed by means of Fourier transform and wavelets. Results show (I) with to respect to the frustum cone that: a) two mean flow structures are formed, one of them is a gas pocket and the other is a bubble cloud. The bubble cloud is produced when the concave meniscus is folded inwards due to fluid flow surrounding that divides the initial gas pocket in two, one remains trapped inside of meniscus area and the other is pushed towards to the cone end. These structures are the main location where the light emission occurs; (II) for the stepped cone that: a) asymmetrical counter-current flows are produced by the stepped boundaries, which generate several stagnation points.

From the detailed analysis of the signals acquired, two issues were found: the frequencies and scales associated with the shock waves emission onset and its propagation, as well as frequency bands in which there is an absence of energy. The detailed flow structures as jets and splashing effects also are considered.

INTRODUCTION

Conical bubble luminescence, CBL, is a procedure in which there are light emissions and the formation of fluid dynamics structures associated with the violent collapse of a conical bubble by means of liquid piston [1–9]. The advantages of the procedure are that solid boundaries tend to stabilize the gas–liquid interface, the heat is transferred between the system and its surroundings through the interface and/or solid boundaries, and the collapse center site is well-defined [2-3]. Furthermore, in conical bubble collapse, CBC renders it viable to control the quantity of the initial volume of the bubble and therefore, the content of the inert gas inside, the concentration of impurities in the liquid piston and, the power of the driving force.

According to radial dynamical models, the collapse time in SBSL (~ ps) and MBSL (~0.5 μs) is shorter than in CBL (~1 ms). This produces a large difference in both, the pressure and temperature reached. Nevertheless, a longer collapse time implies a greater interaction between the inert gas and the atomic and molecular components. Hundreds of chemical reactions can occur within the conical cavity during the timeline of the slow collapse, and the study of these reactions is more feasible in CBL. Most reactions could be chemiluminescent, which would explain the large and bright pulses from CBL compared with the flashes from SBSL and MBSL [9-10].

In the laboratory, cavitation bubbles often are produced by tension on liquids either acoustically or by changing the geometry of the pipeline. Other methods apply the energy focused at a local level within a fluid, either by light bursts / spark discharge or elementary particle collisions [10-12]. Under appropriate conditions, regardless of the method by which the rapid bubble compression is achieved, a light flash is emitted only if a small amount of noble gas is contained in the bubble [13].

In CBC, one more light emission mechanism can be activated depending on the details of collapse, i.e. the timeline during bubble gas-liquid piston interaction. The intensity and shape of the emitted light depend, not only on the initial gas pressure and the driving pressure, but also on the physicochemical properties of the liquid piston and the substances dissolved in it [6-9].

Compression-expansion in CBC, as in other types, is also necessary to understand the fluid dynamics mechanisms responsible for the impulsive forces registered during the collapse. If we consider that in CBC, the gas pocket is completely confined by solid boundaries in its conical part (upper part and body) and the bottom base, the gas liquid interface coupled with the bulk liquid piston forms a thick border which may be considered as an elastic boundary. Therefore, the same phenomena that occur in the cavitation bubble near a rigid wall also apply to CBC.

At least three dynamical mechanisms identify the cavitation bubble near a rigid wall associated with the impulsive forces: shock waves, impinging liquid jets, and splashing effects [14-17]. These papers claim that the main parameter which affects the impulsive behavior is the proximity parameter, γ (the ratio between the distance from the bubble center to the boundary and maximum bubble radius). Experimental observations such as those of Tomita and Shima [18], Blake *et al.* [19] and Lauterborn and Bolle [20] showed that a cavitation bubble almost inevitably fissions itself into many fragments after the first collapse. For a bubble collapsing very close to a solid boundary, a re-entrant jet forms toward the boundary before the bubble reaches its minimum size.

We present the experimental findings on the dynamic in the conical bubble collapse using two conical endings with different geometry. To correlate the light emissions with their dynamical behavior we consider some concepts of the theory that describes the collapsing of a bubble near a rigid boundary.

Frequency and time-frequency theory

The formation and collapse of bubbles are nonlinear processes, and their behavior is time-variant. Therefore, the forces generated and detected in the cone apex, where the bubble collapse takes place, must also be nonlinear and time-variant. The waveforms consequently present variations in energy over time. The wavelet transform based on the Daubechies *Db 10* function is chosen to analyze such variations analysis assuming linearity within the corresponding time window. Nonlinear effects are depicted as variations of the energy among the translated windows. The Fourier transform is employed for the estimation of the featured frequencies of the processes identified by the wavelet analysis.

Analysis in the frequency-domain of a signal $f(t)$ with finite duration is generally realized by means of the Fourier transform (FT). This analysis allows the estimation of the energy contained in a range of frequencies. The corresponding amplitudes $|F(\omega)|$ are an average of the amplitudes present over the duration of the signal. Thus, the FT does not provide any evident information about the time of occurrence of these amplitudes. However, the short-time Fourier transform (STFT) is basically the same FT but estimated for time-translated windows of the signal,

$$F\ w,b\ =\ \int_{-\infty}^{\infty} f(t)s(t-b)^{-i\omega t}dt \quad (1)$$

These windows are represented by a compact-supported function $s(t)$. It is evident that the shape of the window employed will affect the FT estimated. In this study a Hamming window is employed,

$$s\ t\ = 0.54 - 0.46\cos\ 2\pi\frac{t}{T}\ ,\ 0 \le t \le T$$

T stands for the duration of the window. This transform produces FT's associated with each translation b; thus providing a variation of the Fourier spectra over time. Assuming a constant sampling rate, the FT of a shorter signal (a time-windowed signal in comparison to the entire signal) implies that low-frequency information is lost, in addition to a lower frequency resolution. This is also a consequence of using a constant window size in the STFT calculation process.

Wavelet analysis provides a better frequency resolution as the window size is adjusted according to the frequency studied. The wavelet transform is defined as

$$F_w\ a,b\ =\ \int_{-\infty}^{\infty} f\ t\ \frac{1}{\sqrt{a}}\psi\ \frac{t-b}{a}\ dt, \quad a > 0 \quad (2)$$

where a is a variable named scale which defines the size of the window. Scale is inversely proportional to frequency. The equivalency between scale and frequency depends on the function used as basis, which is called wavelet $\psi(t)$. If $\psi(t)$ is defined by a sinusoidal function the equivalency is evident, otherwise this equivalency is subjective and dependent on the fitting of the basis function employed upon a sinusoidal. A discrete form of the expression (2) is herein used and based on the wavelet Db10 (i.e. a wavelet function with 10 vanishing moments) proposed by Daubechies [27]. A detailed description of the FT may be found in many textbooks [28], as well as for the STFT and wavelet analysis [27].

EXPERIMENTAL SET UP

A U-tube apparatus was designed based on the conical device originally employed by other authors as Kosky [1], Hawtin [2], Leighton *et al*. [3], Chen *et al*. [4], and Godinez *et al*, [7-8]. All of them, except the last use a straight conical tip at 30° (equilateral cone). In this case, we use a frustum conical shape and a stepped cone, both with the same height. Figure 1 depicts the layout of experiment; a) it is a diagram of the U-tube apparatus with its measurement equipment, b) shows details of the conical endings. These conical endings were manufactured in polycarbonate with a hexagonal external shape. Table 1 lists the geometric characteristics of both conical endings.

Table 1. Features of the conical endings

Conical endings	Apex ϕ[mm]	Bottom ϕ [mm]	Height [mm]	Volume [cm^3]
Frustum	6.3	25.4	45	10.2 ± 0.1
Stepped	1	26.5	45	05.9 ± 0.1

The bore at the conical apex is sealed by a quartz window and is used then used to fix a piezoelectric transducer (Panametrics centered at 5MHz). Two or three photomultipliers (Hamamatsu, R5783-04 module, PMTs) are settled around the cone to capture the luminescence. The signals from a dynamic force sensor (PCB Piezotronics, ICP 200B05, 75 kHz) and a piezoelectric transducer fixed on the top-plate provided data

about the dynamic oscillating forces caused by the bubble collapse. All signals were captured with a digital oscilloscope (Lecroy, 1 GHz). High speed movies were taken with a Phantom v9.1 camera at framing rate of around 50,000-150, 000 frames per second [fps]. These movies and the transducers outputs are synchronized with the initial displacement of the liquid piston. The acquisition system is triggered by the valve opening that controls the air pressure inlet, B. The fast video acquisition is taken under light and dark room conditions.

The procedure for compressing the gas pocket towards the conical ending is as follows: the U-tube is partially filled with a degasified liquid (1,2 propanediol, 270 ± 10 ml) at room conditions. Subsequently, the free and dissolved air is removed from the system, until a vacuum pressure around 2,500 [Pa] is reached. Next, a small volume of inert gas is injected via arm 1 (See figure 1), filling the free pipe volume, and displacing the liquid into arm 2 (Figure 1). This pressure is measured as a differential height, Δh. At some arbitrary zero time, valve B is opened, thereby allowing air above atmospheric pressure into arm 2, after which the liquid starts to move until the gas collapses on the conical end. The displaced air-liquid interface blocks two laser lines that are separated by 50mm. This data is employed to calculate the liquid piston velocity before it arrives into the tapered portion.

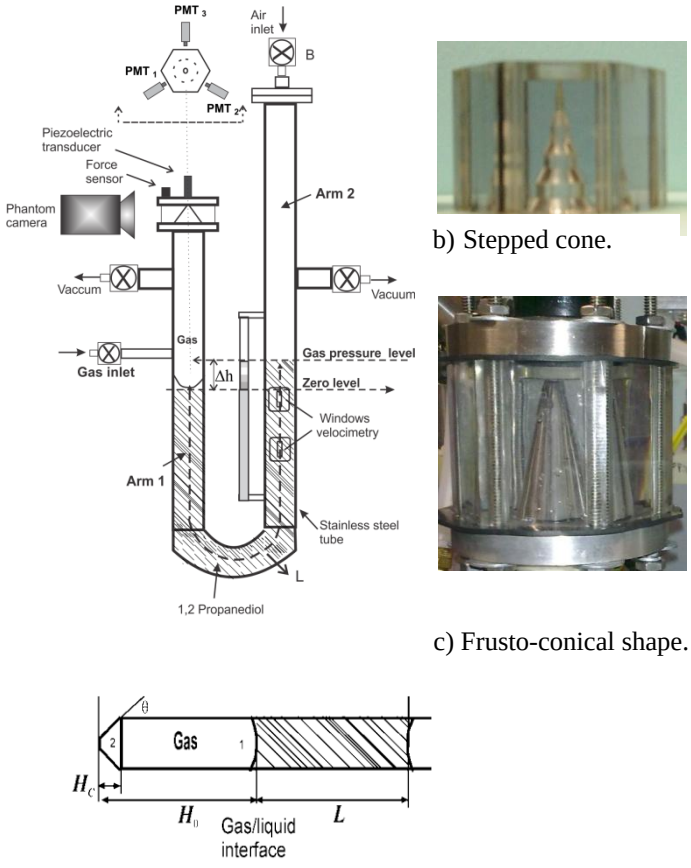

Figure 1 Layout of experiment. Diagram of the U-tube apparatus, which produces the CBC; images of the conical endings; and nomenclature.

The compression, collapse, rebounds, and re-expansion reached the equilibrium after approximately 100ms, during which the remaining gas pocket and liquid are balanced by the external pressure. Liquid piston is added with H_2SO_4 and NaCl powder in small concentrations to increase the light emission brightness.

APPARATUS RESPONSE

The simultaneous record outputs of the U-Tube apparatus are depicted in Figure 2. References [7-8] provide further details. Figure 2a displays representative traces of the transducers: dynamic force sensor, piezoelectric sensor output and light pulse profiles. The dynamic characterization of the device is defined by its predominant frequency, Figure 2b. This frequency is calculated from the coda of the force transducer signal, which corresponds to the free vibration of the device.

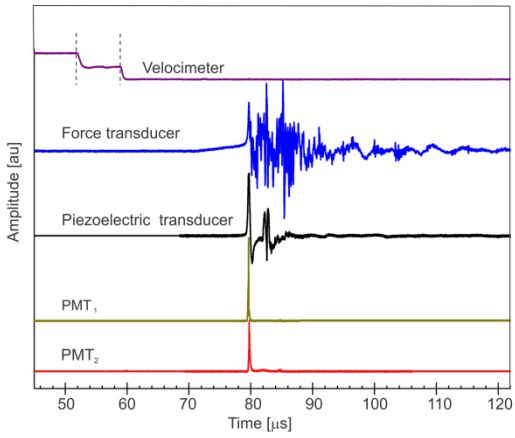

Figure 2a Simultaneous record outputs in CBC

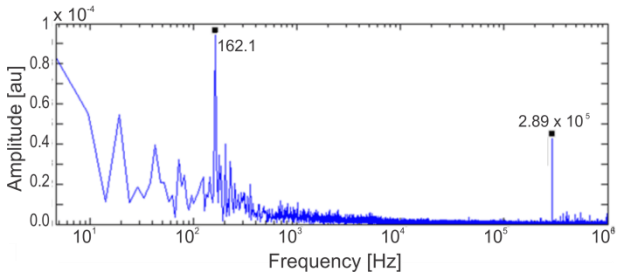

Figure 2b The U-tube resonances

Under the experimental conditions, the U-tube device has two main resonance frequencies around 162 Hz and 289 kHz. The former is due to the oscillatory motion produced by ingress of the air under pressure; the latter is the natural frequency of the U-tube system.

RESULTS

Some typical photographs of the luminescence from CBC by means of liquid piston using two conical endings are shown in Figures 3a to 3b. In these Figures, (a) corresponds to

photographs of the stepped and frustum cone respectively, and b) is a selected frame of light emission obtained by ICCD camera with 8 ms of aperture, in dark room conditions, c) shows light emission profiles detected by a PMT, and d) the first peak of the signals acquired by the dynamic force transducer.

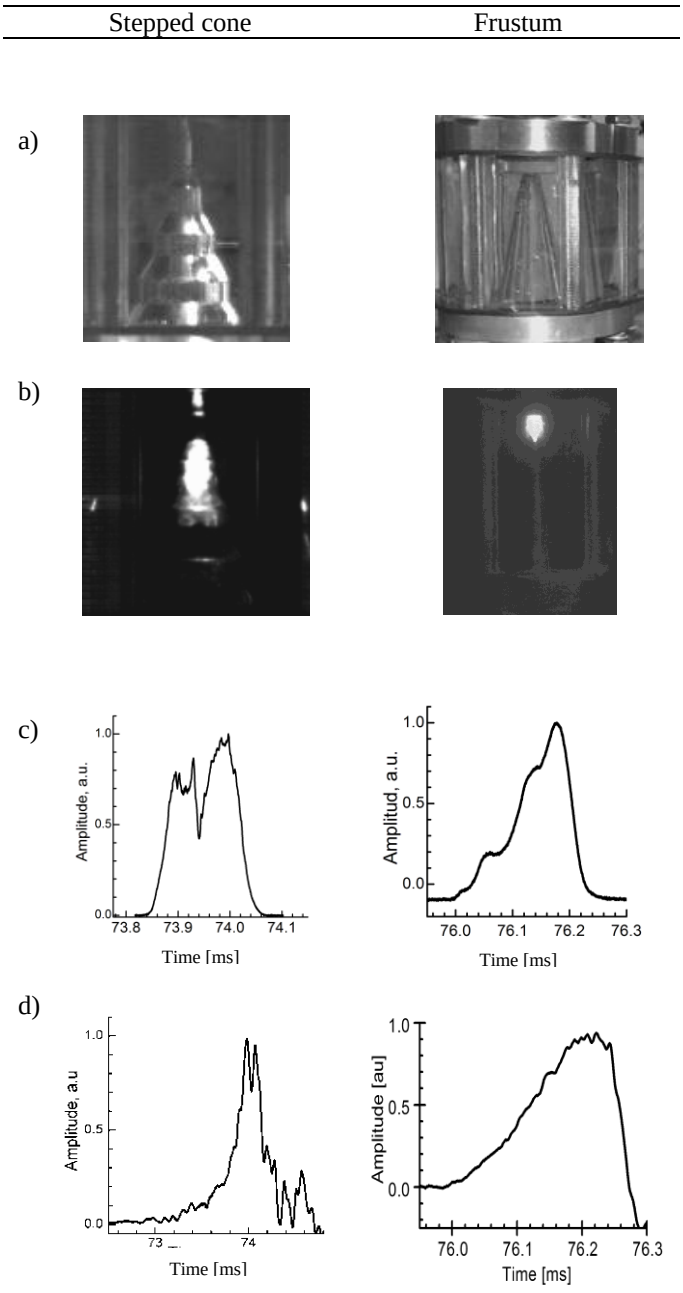

Figure 3 Differences in the dynamics in CBC produced by geometric change of the inside profile of the cone tips. a) images of the conical tips, b) images of the emission of light captured by ICCD, c) light emission profiles captured by PMT, and c) first peak of the signal acquired by the dynamic force transducer

As can be observed, each cone shows distinctive features such as the light emission spots, light pulse profile, and the signal of the force transducer corresponding to the first phase compression. These first results suggest that each one has a distinct dynamic behavior even with identical experimental.

In general, with respect to the emission of light, there are two distinguishing factors: in the frustum cone only one site of light emission is present, at the cone apex location. The PMT profile shows a long pulse, 97.6 μs, formed by three sequential pulses. The compression time lasts about 200 μs.

Regarding the stepped cone behavior, multiple light emission sites occur during the collapse. Its light profile is characterized by broad bands with sharp peaks. Time compression is four times slower than the frustum cone. Furthermore, the stepped geometry decelerates the liquid-piston, the counter-current flow occurs generating local gas pockets. To further explain the light spots, it is necessary to include the dynamics involving shock wave emission, shock wave-bubble interaction, jet formation and its impact, circulation process, ring bubble formation and others fluid dynamic structures. Therefore, it is necessary to correlate both fast video and light emission profiles with the acoustic emission in order to follow these phenomena; this last is shown in Figure 3d.

The results include two main parts: A) Bulk liquid velocity and impulsive forces; B) Temporal force and light pulse vs video frames; C) Data analysis from CBC experimental runs by STFT and wavelets. The experiments include the dynamic tracking of the conical bubble compression/expansion by following the liquid piston meniscus using fast video and by detecting impulsive forces and acoustic emission, as well as the light emission by means of PMTs. All signals are acquired simultaneously and correlated with fast video frames.

A. Bulk liquid velocity and Impulsive forces

As mentioned in the introduction, each experimental run presents unique characteristics. In this subsection the description will be in respect to the experimental run that presents the profiles of the Figures 4 and 5.

The dynamic tracking of compression and expansion during the conical bubble collapse was performed by following a selected point of the liquid piston meniscus through consecutive frames, acquired by a high-speed video camera (Phantom v9.1). The experiments in both conical endings were performed under the same experimental conditions.

Impulse signals generated by the bubble collapse were registered by dynamic force sensors attached on a steel plate on the top of the cone tip. The experimental conditions were Δh= 60 [mm], L=0.5 [m], P_0= 2170 [Pa] (gas vacuum pressure), P_{ext} = 230[kPa] (driving pressure magnitude), liquid density= 1036 [kg/m^3]. The fast-video was taken with the cone fully illuminated for the correct visualization of the liquid displacement. Figure 4 shows the average displacement of the meniscus line for each conical ending. The light pulse onset on the timeline is indicated with an arrow. Figure 5 depicts the impulsive force behavior for each conical ending. The fluid dinamical mechanism is indicated according to the assumptions in references [14–23].

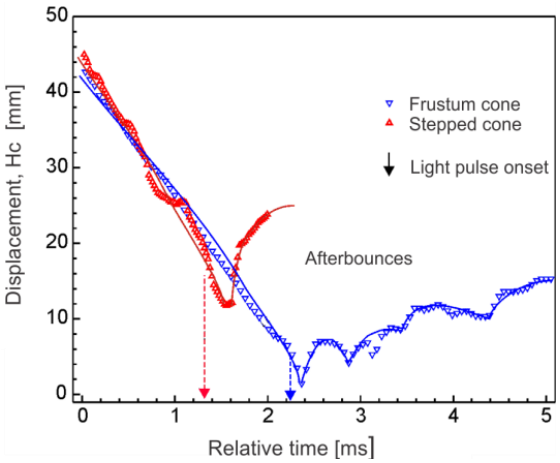

Figure 4 Bulk liquid displacement into the conical endings showing the asymmetrical compression phase and asymmetrical afterbounces. The light pulse onset is indicated by an arrow.

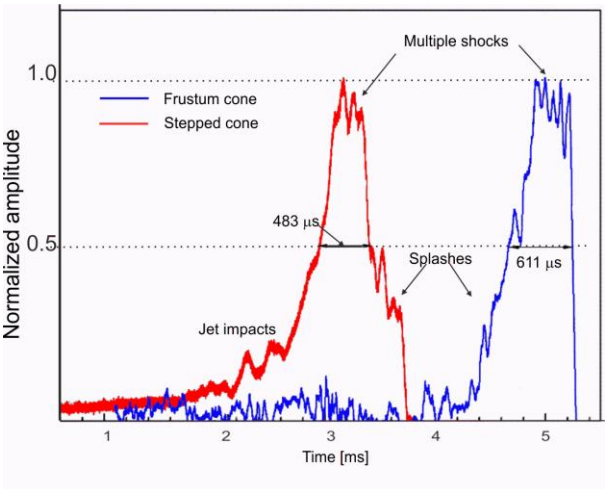

Figure 5 Dynamic force transducer outputs for both conical endings. The light pulse onset is indicated by an arrow. The most likely mechanisms causing the peaks in the signals are listed in this figure, according with references [15-23]

The following subsections briefly describe the dynamics which occur in each conical ending in order to distinguish the main differences.

Stepped cone

The liquid piston reaches the cone base at a rate of 7.18 [m/s] and keeps moving until it reaches 21 [m/s] filling up to the 74% of the cone's volume. As to the cone's tip is very slender, the liquid piston never reaches the tip wall and a portion of gas pocket remains as a plug. However, when the correct compression on the gas is reached, it emits a light pulse. The profile of this emission is shown in figure 3c. In relation to the internal geometry of the cone, the stepped boundaries cause asymmetric flow in countercurrent, which generate several stagnation points. The displacement and the first peak of the impulsive force are drawn with red (stepped cone) and blue (frustum cone) lines in Figure 4 and 5. As shown in figure 4, the frustum cone afterbounces occur more than in the stepped cone, and its light pulse width is more longer.

Frustum cone

During the compression phase, the meniscus of the liquid piston reaches the cone base at a mean rate of 7.15 [m/s], it keeps moving until reaches 17 [m/s], filling the cone up to 85%. The liquid piston compresses the gas pocket in a non-homogeneous form causing a density gradient. At the tip of the cone, the gas is more dense and places further resistence on compression, then a jet is emited from the top, which crosses the gas pocket and perforates the gas-liquid interface forming a hump in the liquid-piston. These statements can be seen in frames 65 to 67 of Figure 6. Now, the gas pocket has two sections. The hump continues to grow and the top gas pocket moves in opossite direction producing a stagnation point. In this case, the initial light emission is generated in the hump inside of the bulk liquid (frame 67). While the hump is still expanding (frames 68-70), the liquid piston continues to compress the gas pocket. A portion of the gas bubble is continuously displacing upwards while the hump is moved in the opposite direction causing a rotation and separation (frames 71-80). Finally, in frames 81to 89 it isseen as an expanding vortex, while a cloud of bubbles is separated.

In this particular case, the maximum compression, the peak force and the onset of light emission almost coincide. The impulsive force and displacement behavior during this experimental run are represented by blue lines in Figures 4 and 5.

The fluid dynamic mechanisms that are specified on the force profiles were indicated by their similarity to the impulsive signals acdquired or calculated by authors [10, 15] who analyzed the behavior of the cavitation bubble collapse near a solid boundary (using focusing laser and high-voltage spark discharge).

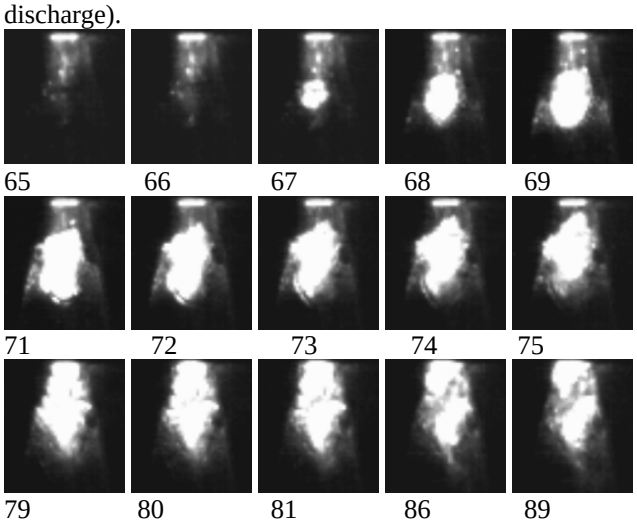

Figure 6 Compresion-expansion in frustum cone. Selecting frames from high speed-video. Each frame was taken at 33.25 µs of exposure time

Extrapolating the analysis on impulsive forces which are generated by cavitation bubble collapse near a solid boundary

carried out by authors in references [15-23], we presented our own assumptions with respect to CBC: the collapse is strongly asymmetric, as it is observed in the afterbounces, the force shapes and the light emission profiles: the collapse resembles a cloud bubble near several solid boundaries; at least one or more stagnation points may be formed; the maximun compression does not always coincide with the light emission; and two sources of light may be involved during the emission: a) thermal-chemical, and b) plasma in the breakdown channel in liquid.

B. Temporal force and light pulse vs video frames

In this section, the light emission acquired by means of PMTs, the impulsive force and high-speed video in dark room conditions are matched on the same timeline.

Frustum cone

In the large cone, (Figure 7), everything appears to happen at the top. However the force and the emission profiles contradic this assumption, and show analogous results to those descibed in Figure 6. Frames 3 to 6 show a black spots, which are believed to be the density change due to liquid jet flow. In this case, there is only one location for light emission at the top.

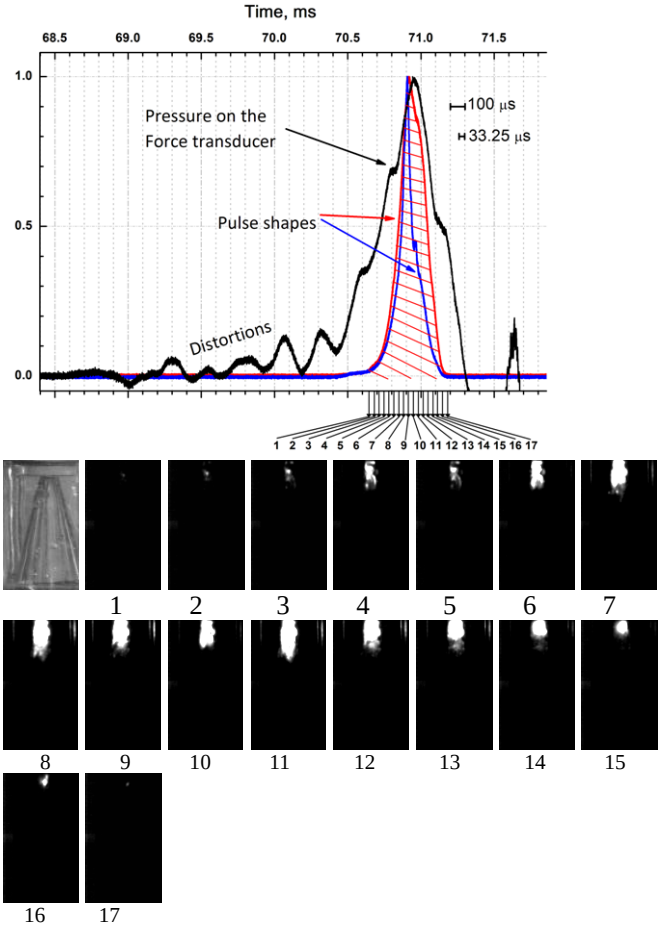

Figure 7 Variation of the pressure and light pulses as a function of time mached to light emission photographs using a large conical tip

Stepped cone

As shown in the frames, in the Figure 8, the light pulse onset occurs at the middle of the cone and expands toward the top increasing its brightness (frames 1 to 6). In this process, the gas pocket loses kinetic energy, and the liquid piston compresses it, again and reaches the slender tip (frames 10 to 12).The following frames (7 to 21) show a wake of light that fades until disappearing. The dynamic force and light profiles (see frame 1) describe the dynamical mechanism, under which the conical bubble was subjected. This is observed in the plots, wherein the PMT is located at the middle of cone, capturing the light (blue line). The maximun peak force appear 100 µs after. The double peak and distortions which the force profile displays are associated with the formation of a ring bubble that is attached to a vortex sheet, starting from the first collapse of the conical bubble, see reference [19, 25].

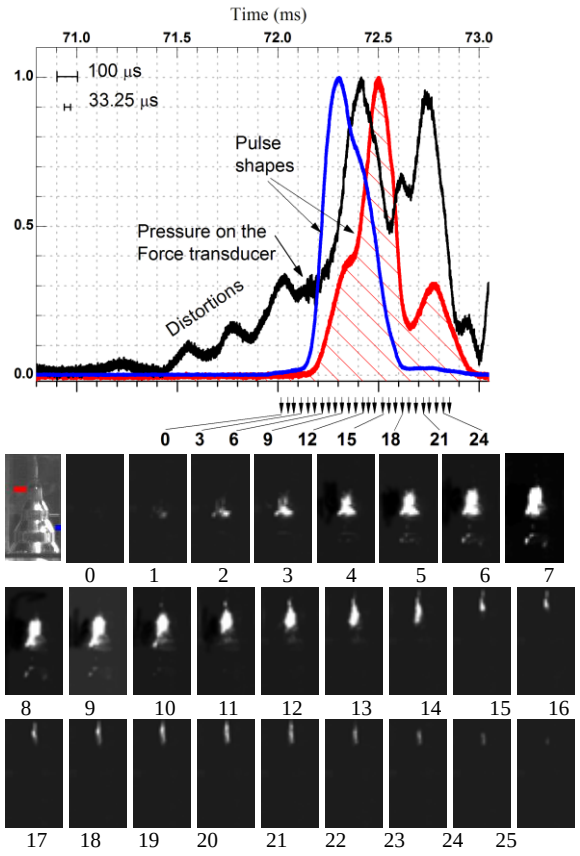

Figure 8 Variation of pressure and pulse light as a function of time matched to light emission photographs, using a stepped conical end.

C. Analysis dynamic stages by STFT and wavelets

Analysis of the acquired waveforms can reveal different phenomena which were not identified in high-speed video, such as the main shock wave emitted during the compression stage. The analysis of the signals obtained during an experimental run with the aforementioned conditions is herein presented**.** Figure 9 shows a window of the piezoelectric transducer signal (Figure 2a) which includes the interval of time when the light

pulses are registered by the PMTs. This signal is analyzed by short-time Fourier (STFT) and wavelet transforms (WT). This latter is further analyzed with Fourier transform (FT) in order to associate frequencies of the piezoelectric transducer signal with the conical bubble collapse using the frustum cone. The STFT is employed for the time-frequency analysis of the windowed signal. The STFT is based on a 67 μs Hamming window, overlapping 50% of such window. The STFT obtained and the force signal analyzed is shown in Figure 9.

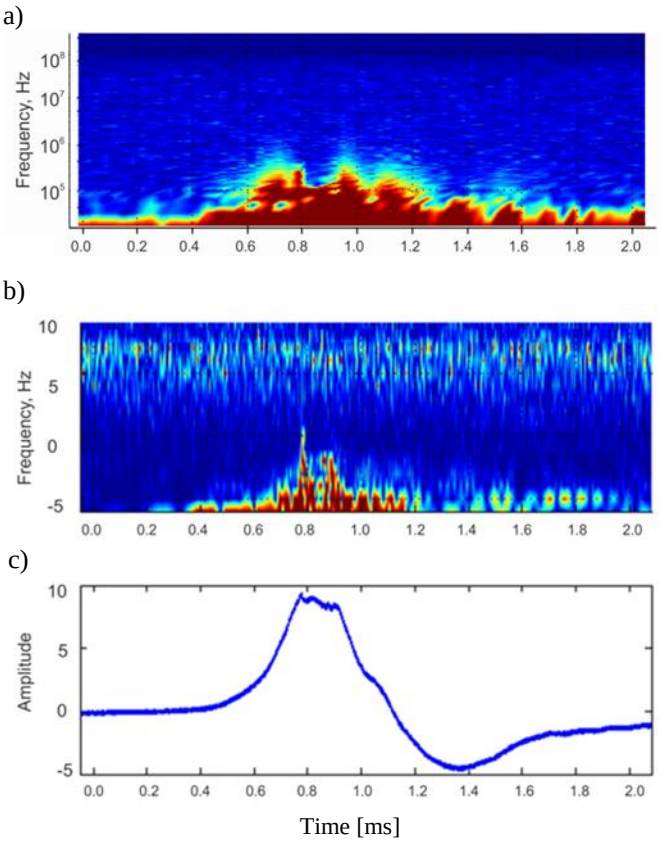

Figure 9 (a) STFT of the windowed piezoelectric transducer signal (c), and b) absolute value of the scales time-history produced by the wavelet.

The existence of shock waves is physically detected when light is emitted. The occurrence of characteristic energy at a particular range of frequencies between 100 kHz to 500 kHz is observed. This high-frequency energy may be related to such identified shock waves.

A wavelet analysis is performed on the piezoelectric transducer signal in order to filter and further isolate the frequencies corresponding to the shock waves. The discrete wavelet analysis is based on one of the functions proposed by Daubechies (Db_10). The representation of the wavelet transform employs the corresponding time-history of the different scales produced, as they have a better time-location than the corresponding coefficients of the wavelet transform. Figure 9b presents the absolute value of the time-history of the scales produced by the wavelet analysis of the force signal.

The energy manifested around scales 6-10 may be associated with shock waves as they both occur at the same time (at 800 μs). As opposed to the variations present in other scales observed in the time window shown in Figure 9b, the variations occurring in scales 6-10 are present only during the propagation of shock waves.

This is shown in Figure 10, which presents the time-history of the highest frequency scales influenced by the shock waves.

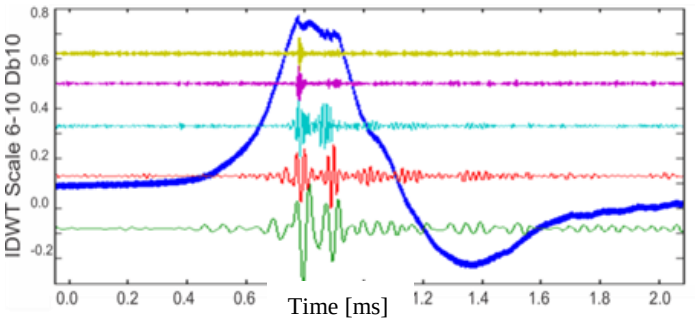

Figure 10 Time-history of the scales 6 (green line) to 10 (light green line), as well as the corresponding piezoelectric transducer signal (blue line) are shown

For the time window analyzed, it is reasonable to characterize the occurrence of the shock waves with the time-history of the scales 6-10. It can be seen that fluctuations in time-history of scale 9 – 10 mainly detect the onset of the shock wave propagation. Scales 6-8 nearly identify the shock wave propagation. These scale time-histories are further analyzed by FT. A directly proportional decrease of the fundamental frequency to the number of scale is observed. It is reasonable to associate this range of frequencies with the occurrence of shock waves, as they identify such waves in time domain. This range is defined roughly from (15 to 600 kHz), which is consistent with the range obtained by STFT. Moreover, the onset of the shock waves may be related with the corresponding frequencies of the scales 9 – 10 (100 – 600 kHz), while the duration of the shock waves may be identified by the range associated with the scales 6 – 8 (15 – 150 kHz).

DISCUSSION

The possibility of obtaining a light pulse from another source (that is neither thermal nor chemical) is to ensure that the system generates a liquid jet with sufficient energy to punch the interface and collide with a bulk liquid wall. The assumption is based on the well-known physical effect of double electric layer, which appears in liquid near to a liquid-gas boundary surface. Deformation of this layer under an asymmetric jet generates an electric field inside the bubble and an electric breakdown may occur under certain conditions [26].

In accordance with the findings of numerous authors (see references [8, 9]), one or more light emission mechanisms can be activated depending on the details of the collapse. The intensity and shape of the emitted light depends on the initial gas pressure, driving pressure and physicochemical properties of the host liquid and the substances dissolved in it, and now it adds other: the geometrical boundaries. This condition opens the possibility of more contributions to light emission.

CONCLUSION

A study of dynamics of the conical bubble collapse using a liquid piston was realized. The behavior of the compression/expansion and light emission was observed by means of high-speed video, along with measurements of impulsive force and shapes of light pulses. As a result, some interesting phenomena have been experimentally observed. For instance, a) the compression/expansion and rebound are asymmetrical; b) displacement of the interface shows asymmetrical rebounds and the velocity calculated from it is very slow compared with SBL or MBSL; c) the light pulses and impulsive forces shapes, as well as the frames from high speed video -indicate temporal and spatial separation among sites of-light emission. It must be pointed out that: there is a generation of stagnation points during the compression and expansion phases, such as these sites are favored as light emitting locations. Furthermore, we find the energy associated with shock waves using wavelet analysis of the acoustic signal acquired by a piezoelectric transducer.

The CBC is very asymmetric and strongly nonlinear. Each conical end presents different dynamical stages. Nevertheless, we can affirm that when the bubble gas compresses towards its minimum volume, there are conditions to produce the light emission by thermal mechanism (considering adiabatic or isothermal compression) and also light emission by chemical reactions, but as a result of the increase in temperature. In these experimental runs another possibility is now open: the plasma formation in breakdown of the liquid channel.

In summary, several light-emission mechanisms can occur in the conical bubble collapse: thermal, chemical as well by electrical processes.

ACKNOWLEDGMENTS

The authors gratefully acknowledge financial support from UNAM-DGAPA-PAPPIT under Grant IN105212-3, II-FI-UNAM under Grant 1135, 2108 and 3130 from UNAM-II.

REFERENCES

[1] Kosky, P. G., Bubble growth measurements in uniformly superheated liquids, *Chem. Eng. Sci.*, Vol. 23, 1968, pp. 695-706

[2] Hawtin, P., Henwood, G. A., and Huber, R. A., On the collapse of water vapor cavities in a bubble analogue apparatus, *Chem. Eng. Sci.*, Vol. 25, 1970, pp. 1197-1209

[3] Leighton, T.G., Cox, B., Phelps, A.D., The Rayleigh-like collapse of a conical bubble, *J. Acoust. Soc. Am.*, Vol. 107, 2000, pp. 130-142

[4] Chen, Q. D., Fu, L.M., Ai, X. C., Zhan, J. P., Wang, L., Ultrabright cavitation luminescence generation and its time-resolved spectroscopic characterization, *Phys. Rev. E.*, Vol. 70, 2004, pp. 047301

[5] He, S.J., Ai, X.C., Dong, L. F., Chen, D.Y., Wang, O., Li, X.C., Zhan, J.P., Wang, L., Conical bubble photoluminescence from rhodamine 6G in 1,2-propanediol, *Chin. Phys*., Vol. 15, 2006, pp. 1615-1620

[6] Jing, H., He, S. J., Fang, W., Min, S. J., Cavitation luminescence of argon-saturated alkali-metal solutions from a conical bubble, *J. Phys. B: At. Mol. Opt. Phys*., Vol. 41, 2008, pp. 195402

[7] Xu, H., Eddingsaas, N. C., Suslick, K. S., Spatial separation of cavitation bubble populations: the nanodroplet injection model, *J. Am. Chem. Soc.*, Vol. 131, 2009, pp. 6060-6061

[8] M. Navarrete, Sanchéz C, Godínez F A, Mejía E V, Villagrán M., Luminescence features from conical bubble collapse in 1,2 propanediol and its perturbation adding sulfuric acid *J. Phys.: Conf. Ser.*, Vol. 274, 2011, 012095, 18 pp.

[9] Godínez, F. A., Navarrete, M., Sánchez-Ake, C., Mejía, E.V., Villagrán, M., Spectroscopic and thermodynamic features of conical bubble luminescence, *Ultrasonics Sonochemistry*, Vol. 19, 2011, pp. 2668-681

[10] Ohl, C. D., Probing luminescence from nonspherical bubble collapse, *Phys. Fluids*, Vol. 14, 2002, pp. 2700-2708

[11] Harvey, E. N., Sonoluminescence and sonic chemiluminescence, *J. Am. Chem. Soc.*, Vol. 61, 1939, pp. 2392–2398

[12] Khodorkovskii, M.A., Murashov, S.V., Artamonova, T.O, Rakcheeva, L. P., Excitation of water molecules by electron impact with formation of OH^{o} radicals in the A2 + state, *J. Phys. B: At. Mol. Opt. Phys.*, Vol. 42, 2009, pp.215201-215206

[13] Rayleigh, L. 1917, "The pressure developed in a liquid on the collapse of a spherical cavity," *Philos. Magn*., 34, 94-98.

[14] Brennen, C. E., Cavitation and Bubble Dynamics, *Oxford University Press, New York, NY.* 1995

[15] Tong, R.P., Schiffers, W. P., Shaw, S. J., Blake, J. R., Emmony, D.C., The role of splashing in the collapse of a laser-generated cavity near a rigid boundary, *J. Fluid Mech.*, Vol. 380, 1999, pp. 339-361

[16] Takayama, S. K., Tomita, Y., Mechanism of impact pressure generation from spark-generated bubble collapse near a wall, *AIAA J*, Vol. 21 (1), 1983, pp. 55-59

[17] Lauterborn W., Cavitation erosion by single laser produced bubbles, *J. Fluid Mech.*, Vol. 361, 1998, pp. 75-116.

[18] Tomita, Y., Shima, A., High-speed photographic observations of laser induced cavitation bubbles in water *Acustica*, Vol. 71, 1990, pp. 161-171

[19] Blake J. R., Tomita Y., and Tong R. P., The art, craft and science of modelling jet impact in a collapsing cavitation bubble, *Applied Scientific Research*, Vol. 58, 1998, pp. 77-90

[20] Lauterborn W., Bolle H., Experimental investigations of cavitation bubble collapse in the neighborhood of a solid boundary, *J. Fluid. Mech.*, Vol. 135, 1975, pp. 373-387

[21] Wang, Yi-Chun, Chen, Yu-Wen., Applications of piezoelectric PVDF film to the measurement of impulsive forces generated by cavitation bubble collapse near a solid boundary, *Experimental Thermal and Fluid Science*, Vol. 32, 2007, pp. 403-414

[22] Ohl, C. D., Ikink, R., Shock-wave-induced jetting of micron-size bubbles," *Phys. Rev. Lett.*, Vol. 80, 2003, pp. 214502-1-214502-4

[23] Duncan, J.H., Zhang, S., Chahine, G. L., The final stage of the collapse of a cavitation bubble near a rigid wall, *J. Fluid Mech.*, Vol. 257, 1993, pp. 147-181

[24] Tomita, Y., Interaction of a shock wave with a single bubble, *Shock wave science and technology, part 1*, 200, pp.35-66.

[25] Konno, A., Kato, H., Yamaguchi, H. and Maeda, M., Observation of Cavitation Bubble Collapse by High-speed Video," *Proceedings of The Fifth Asian Symposium on Visualization*, Vol.1, 1999, pp. 134-139.

[26] Borissenok, V.A., Sonoluminescence: Two sources of light, *Physics Letters A*, Vol. 372, 2008, pp. 3496-3500

[27] Daubechies I, Ten lectures on wavelets, *Rutgers University and AT&T Bell laboratories*, Society for industrial and Applied mathematics, Philadelphia, Pennsylvania, 1992.

[28] Lathi B. P., *Signal Processing and Linear Systems*, Berkeley – Cambridge Press, Carmichael, CA, 1998.